crystals

MDPI

Article

Unmodified Titanium Dioxide Nanoparticles as a Potential Contrast Agent in Photon Emission Computed Tomography

Awais Khalid [1,2], Pervaiz Ahmad [2,3,*], Abdulrahman I. Alharthi [4], Saleh Muhammad [1], Mayeen Uddin Khandaker [5], Mohammad Rashed Iqbal Faruque [6], Israf Ud Din [4] and Mshari A. Alotaibi [4]

1 Department of Physics, Hazara University Mansehra, Khyber Pakhtunkhwa 21300, Pakistan; ask4awais@gmail.com (A.K.); saleh.dagiwal@gmail.com (S.M.)
2 Department of Physics, Faculty of Science, University of Malaya, Kuala Lumpur 50603, Selangor, Malaysia
3 Department of Physics, University of Azad Jammu and Kashmir, Muzaffarabad 13100, Pakistan
4 Department of Chemistry, College of Science and Humanities, Prince Sattam Bin Abdulaziz University, P.O. Box 173, Al-Kharj 11942, Saudi Arabia; a.alharati@psau.edu.sa (A.I.A.); i.din@psau.edu.sa (I.U.D.); alosaimi@psau.edu.sa (M.A.A.)
5 Center for Applied Physics and Radiation Technologies, School of Engineering and Technology, Sunway University, Bandar Sunway 47500, Selangor, Malaysia; mayeenk@sunway.edu.my
6 Space Science Centre, Universiti Kebangsaan Malaysia (UKM), Bangi 43600, Selangor, Malaysia; rashed@ukm.edu.my
* Correspondence: pervaiz.pas@gmail.com or pervaiz.ahmad@ajku.edu.pk; Tel.: +92-345-9493879

Abstract: Highly crystalline titanium dioxide nanoparticles (TiO_2-NPs) are synthesized via a simple hydrothermal technique. After structural and compositional analysis, the as-synthesized unmodified TiO_2-NPs are tested for improvement in two modes of kilovoltage radiation therapy and single-photon emission computed tomography (SPECT)/computed tomography (CT). Our results show that the unmodified TiO_2-NPs provide an observable enhancement in CT scan image contrast ranging from 0 ± 3 HU (without NPs) to 283.7 ± 3 HU (0.23 g/mL). TiO_2-NPs has excellent biocompatibility, selective uptake at target sites, and reduced toxicity. The unmodified TiO_2-NPs as a contrast agent can significantly improve the existing methods of diagnosing and treating cancer.

Keywords: nanoparticles; titanium dioxide; highly crystalline; computed tomography

Citation: Khalid, A.; Ahmad, P.; Alharthi, A.I.; Muhammad, S.; Khandaker, M.U.; Iqbal Faruque, M.R.; Din, I.U.; Alotaibi, M.A. Unmodified Titanium Dioxide Nanoparticles as a Potential Contrast Agent in Photon Emission Computed Tomography. *Crystals* **2021**, *11*, 171. https://doi.org/10.3390/cryst11020171

Academic Editor: Leonid Kustov
Received: 10 January 2021
Accepted: 3 February 2021
Published: 9 February 2021

1. Introduction

Titanium dioxide nanoparticles (TiO_2-NPs) are among the most widely used engineered nanostructures of TiO_2. Most of the TiO_2 applications are due to their structural and electronic properties. It consists of mainly three phases which included anatase, rutile, and brookite [1]. Due to its greater photocatalytic activity [2], anatase has the highest number of industrial applications compared to rutile and brookite [3]. At the beginning of the 20th century, mass production of TiO_2-NPs started as a non-toxic substitute for a white dye used in paints. It has various applications in food colorant or white pigment in manufacturing plastics, paper, ink, paints, and welding rod coating material. Ultrafine TiO_2-NPs [4] are widely used in other industrial products, such as cosmetics, toothpaste, pharmaceuticals, and skincare products [3,5–7]. TiO_2-NPs is an n-type semiconductor with a wide bandgap, having various applications in wastewater treatments dye-sensitized solar cells, photoionized devices, and lithium batteries [8]. TiO_2-NPs have specific medicinal properties and have been used in many biomedical applications such as artificial hips, dental implants, bone plates, coatings, scaffolds, and also in gene and drug delivery systems.

Interest in the synthesis of TiO_2-NPs and their applications are due to their biocompatibility [9–11], antimicrobial properties [12,13], high chemical stability, specific surface area, and catalytic activity [14–16]. Because of the wide range of applications, TiO_2-NPs have considerable potential for human exposure. People can be exposed to these nanoparticles through oral, respiratory, or dermal routes. TiO_2-NPs have been used in the food

industry since 1996 when the US Food and Drug Administration approved it as a food supplement [17]. TiO_2-NPs are also used for electrostatic properties in terms of electrostatic potentials and ion distributions [18] for dye-degrading activities, H_2O_2 scavenging, and anticoagulant activities [19] to enhance the glasses' radiation protection properties along with bioactive glasses [20] as nanocarriers for drug delivery [21] and as a nano-drug for treating diseases [22]. The idea of agents for two modes of therapy enhancement and image contrast is one field that remains largely unexplored. The principle of two modes of enhancement agents has been validated for radiotherapy enhancement applications by using conventional non-nanoparticle image contrast agents such as iodine [23–25].

There have been reports in which TiO_2-NPs can be used in radiation therapy applications for the treatment of cancer due to their absorptive properties and higher refractive index [23–26]. The tumor during radiotherapy is exposed to ionizing radiation. As a result, it gives damage to the DNA of the tumor and other biological molecules and ultimately results in the cell's death.

The inescapable radiation dose administered to the surrounding healthy tissues of the tumor being treated is the intrinsic drawback of radiation therapy. The use of radiotherapy is restricted for some tumors, due to unwanted damage to the surrounding healthy tissue by the dose required to destroy the tumor [27]. Cheng et al. investigated a hybrid anisotropic nanostructure, composed of gold (Au) doped titanium dioxide (TiO_2), as a radio-sensitizer for radiotherapy of triple-negative breast cancer (TNBC) [28]. Liang et al. used TiO_2 to enhance the quantum yield in ultra-sound activated sonodynamic therapy (SDT) [29]. Yang et al. synthesized carbon-doped titanium dioxide to generate ROS to eliminate tumor cells under ultrasound irradiation [30]. Su et al. construct an active site in a TiO_2 nano catalyst by auger electrons (AEs) for cancer catalytic internal radiotherapy (CIRT) applications [31]. Contrast-enhanced radiotherapy (CERT) [32] requires injection of contrast agents to the target volume with high-Z (high atomic number) and kilovoltage X-rays irradiation. Since materials with a high Z content have different absorption properties from those of healthy tissues, therefore the distribution of the absorbed dose can be changed due to their presence. In areas where a contrast agent is present, an increase in localized dose can be obtained without affecting the healthy tissue [23,24]. Kilovoltage X-rays energy range is considered the ideal range for CERT [24] because the change in photo absorbing properties is noticeable at kilovolt energies [32,33]. Some improvement has also been observed in contrast by using X-ray energy in the megavolt range provided by medical linear accelerators (Linac) [34,35]. TiO_2-NPs with a size in the range of smaller than 100 nm can penetrate the cell membrane and preferably accumulate in cancer cells [36]. Moreover, it can work as the required contrast agent.

Previously iodine has been used as a contrast agent for computed tomography (CT) imaging [37]. A conventional CT scanner was used to monitor iodine uptake and tumor progression simultaneously. The pioneer studies for photodynamic therapy and MRI enhancement have missed or ignored the concept of nanoparticles-based enhancement agents [38,39]. NPs synthesized for radiotherapy and ionizing radiation would be beneficial to monitor them with CT scanners as it is the standard imaging tool for treatment planning and diagnosis [40,41]. These CT scanners are gradually replacing the conventional radiotherapy treatment planning simulator units. A conventional CT scanner may also be updated to deliver therapeutic doses of X-rays by using iodine CERT [24,41]. The dose distributions generated by this method is comparable to those obtained with 10 MV therapy and allows simulation, hybrid imaging, and treatment on a similar mechanism [24]. A similar alternative would be highly desirable for more advanced contrast agents.

This alternative can be sought with TiO_2-NPs because it has the potential to be used as a contrast agent, radiotherapy enhancement agent, and have an anti-cancer effect. Although various studies have examined the imaging properties of chemically modified TiO_2-NPs, the imaging properties of unmodified TiO_2-NPs have not been studied. Thus, the current study is based on the visibility of unmodified TiO_2-NPs (synthesized by hydrothermal

route) by using CT and kilovoltage X-ray unit to determine their image contrast and radiation enhancement properties.

2. Materials and Methods

TiO_2-NPs have been synthesized by using 3 g of commercial titanium dioxide (in bulk). At room temperature, the bulk TiO_2 is mixed with 80 mL of sodium hydroxide (from 10 M aqueous solution) by vigorous stirring for 1.5 h. Afterward, it is placed in a Teflon-lined autoclave and heated at 160 °C for 48 h. The resulting precipitate after cooling down at room temperature is washed several times with diluted hydrochloric acid (0.1 M) and deionized water and then dried at 120 °C in the oven for 2 h. The imaging capabilities of the synthesized TiO_2-NPs were investigated by inserting its solution at 1.5 cm depth with the help of a cylindrical vial. Discovery NM/CT 670 pro (GE Healthcare) was used to image these vials and the CT values of each vial are provided in Hounsfield units (the standard unit for CT scans) [42]. The resulting values and concentration are plotted to obtain a linear fit. The solutions on a WOmed T-200 kilovoltage X-ray therapy unit are exposed to test their dose enhancement competencies. The solutions are mounted on the phantom's surface in plastic tubes so that the thickness of the nanoparticle solution was 0.5 cm. Radiation-sensitive radio chromic film (Gaphchromic EBT2) was positioned on the solution's surface in such a way that the radiation source was facing the active sheet. The film was then exposed to the surface with a dosage of 1.00 Gy. To determine whether the existence of nanoparticles enhances the dose, the dose reported by each piece of film was plotted against the concentration of the nanoparticle.

3. Results

A field emission scanning electron microscope (FE-SEM) is used to observe the apparent morphology of the as-synthesized TiO_2-NPs. The obtained information about the structure or morphology of the as-synthesized TiO_2-NPs is shown in Figure 1. All the TiO_2-NPs seem like small spheres (nanospheres). The micrograph shows that almost all of the TiO_2-NPs are in the nanometer range. At the bottom, most of the smaller size particles are closely packed alongside others. The smaller the size of the particle, the more at the bottom it lies followed by a bit bigger, etc. In contrast, at the top, the larger size particles are mostly seemed isolated from one another. It is an indication of the top-down approach followed during the synthesis of TiO_2-NPs. Nanoparticles of different sizes (smaller and bigger) can be seen and observed in the current micrograph. Thus, the biggest particles in the sample are placed at the top followed by the smaller and smallest at the bottom. This observation further verifying the top-down approach followed during the synthesis of TiO_2-NPs. The FE-SEM results show that the average particle size is below 100 nm.

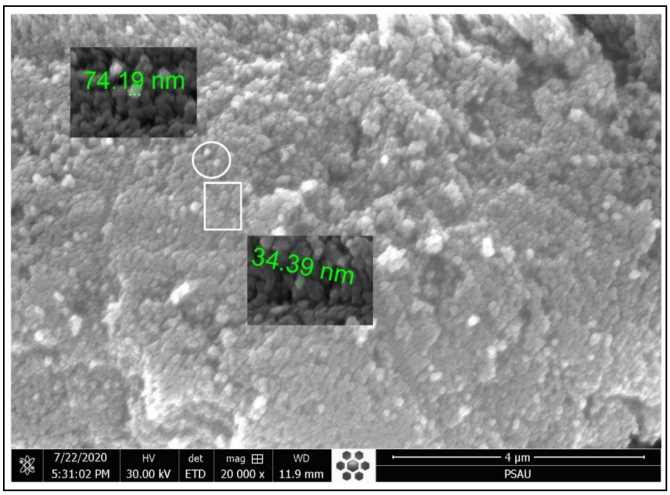

Figure 1. Field emission scanning electron microscope (FE-SEM) micrograph of the as-synthesized titanium dioxide (TiO_2) nanoparticles.

X-ray diffraction pattern of the as-synthesized TiO_2-NPs is shown in Figure 2. It is an analytical technique used to identify the crystallinity and phase formation of TiO_2-NPs. The XRD study was conducted through the X-ray diffractometer at 298 K by using a nickel-filtered Cu α radiations source (K = 1.5418) at 298 K. The intensity data was attained over a 2θ range of 10–80°. The diffraction peaks were observed at the diffraction angle of 23.17°, 25.71°, 27.92°, 36.57°, 37.53°, 38.32°, 41.71°, 48.52°, 54.46°, 55.51°, 57.09°, 69.30°, 70.71°, and 75.48°, respectively. The crystalline phases of TiO_2-NPs were identified by X'Pert high score by comparing it with the standard data JCPDS card no. 01-075-1537 (Anatase) and 01-082-0514 (Rutile). Accordingly, all the peaks correspond to (101), (110), (103), (004), (112), (111), (200), (105), (211), (220), (116), (220), and (202) planes in the as-synthesized TiO_2. Debye Scherrer equation was used to measure the crystallite size of the synthesized nanoparticles with the help of XRD data of all the prominent peaks according to which the average crystallite size of TiO_2-NPs was 20 nm.

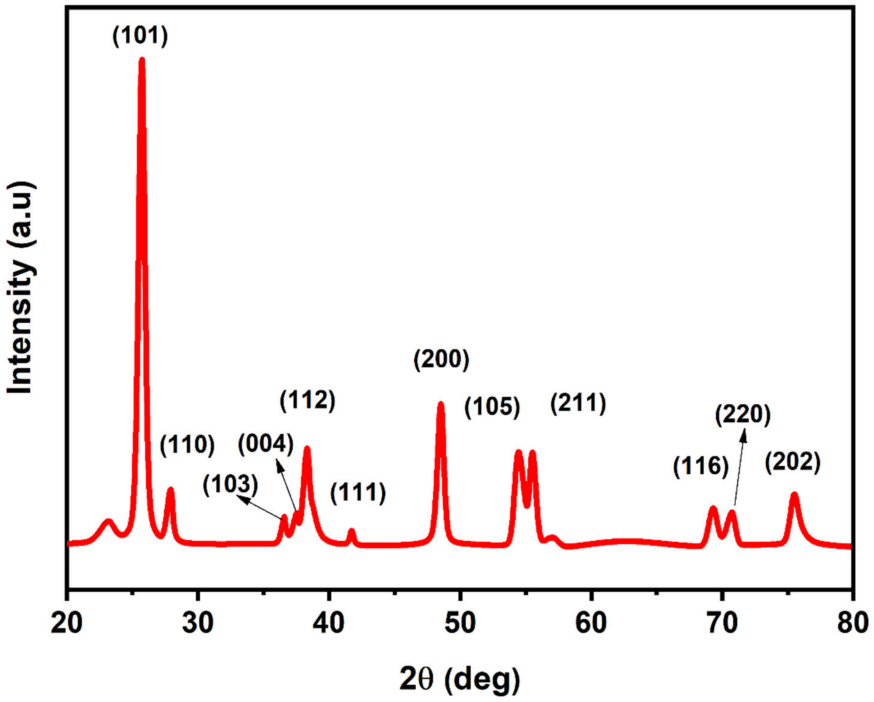

Figure 2. X-ray diffraction pattern of TiO_2.

Bonding properties, valence states, and quantitative analysis of the electronic structures of the synthesized TiO_2-NPs were performed by X-ray photoelectron spectroscopy (XPS). In the XPS analysis, Ti 2p and O 1s are observed and no other precursor elements or magnetic contamination are found as shown in Figure 3. Moreover, the hydrocarbon contamination (C 1s) peak is detected at approximately 285 eV [43]. The XPS survey with the peaks tagged for the corresponding elements for their binding energies is shown in Figure 3a. Two sharp peaks are observed in Figure 3b, which corresponded to the spin-orbit of Ti $2p_{3/2}$ and Ti $2p_{1/2}$ at binding energies of 463 eV and 468 eV for Ti^{4+} in TiO_2. No obvious peak shift is observed. This shows that Ti atoms exist in the same oxidation state [44]. The magnified O 1 s peak is shown in Figure 3c. The peak observed at 533 eV is interpreted to be due to bulk oxygen in the TiO_2 [45]. The full width at half maximum (FWHM) is approximately similar in all spectra (1.35 eV). In Figure 3a, escorting to the higher binding energy side of the peak involves many components resulting from TiO_2 surface hydroxylation (when it is mounted the electrode is exposed to air). These are attributable to both acidic and fundamental hydroxyl groups and absorbed water at the outermost surface. We observe the O 1s spectrum similar to those recorded on untreated (as grown) single crystal of anatase [46] and rutile exposed to vapor and liquid water [47,48].

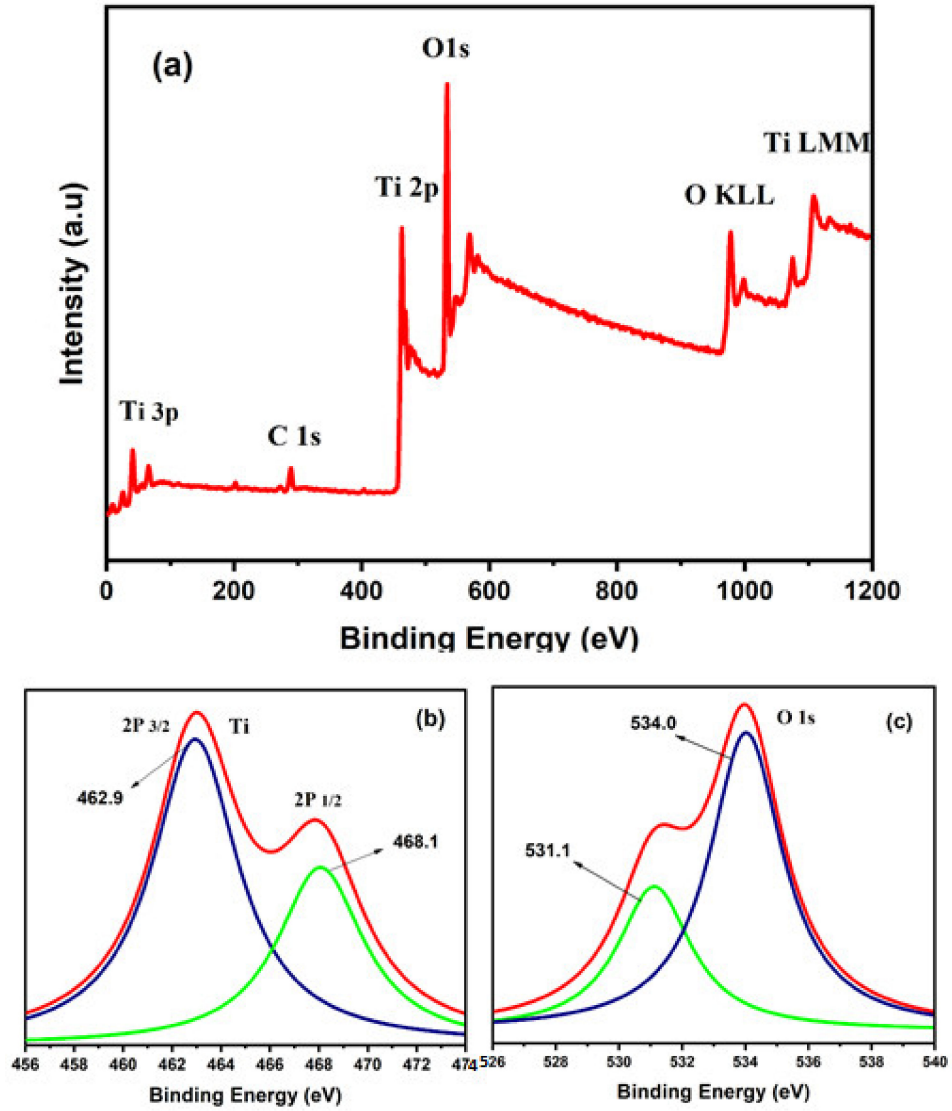

Figure 3. (**a**) XPS survey of the as-synthesized TiO_2 nanoparticles, (**b**) high-resolution Ti 2p, and (**c**) O 1s XPS spectra.

Figure 4 shows the Raman spectrum of the as-synthesized TiO_2-NPs. The intense E_g mode appears at 143.7 cm^{-1} [49]. B_{1g}, (A_{1g} + B_{1g}) and E_g peaks appear at 399 cm^{-1}, 516 cm^{-1}, and 637 cm^{-1} respectively. In TiO_2 vibrational modes are due to the symmetric, asymmetric, and bending vibration of the Ti–O–Ti bond [50,51]. The peak tagged by Eg stands for Ti–O stretching mode, whereas the peaks located at 516 cm^{-1} and 399 cm^{-1} modes refer to Ti–O stretching mode (the only O is moving) and O–Ti–O bending mode (Ti is moving) [51,52]. Phonons near the center of the Brillouin zone (BZ) contribute to the inelastic dispersion of incident radiations only in a perfect infinite crystal. A greater part of the BZ will efficiently participate in scattering processes as the size of the crystal vary in the nanoscale due to the weakening of the selection rule at $q_0 \approx 0$. Thus, a change in the Raman frequency peaks and the shape of the Raman band can be observed [53].

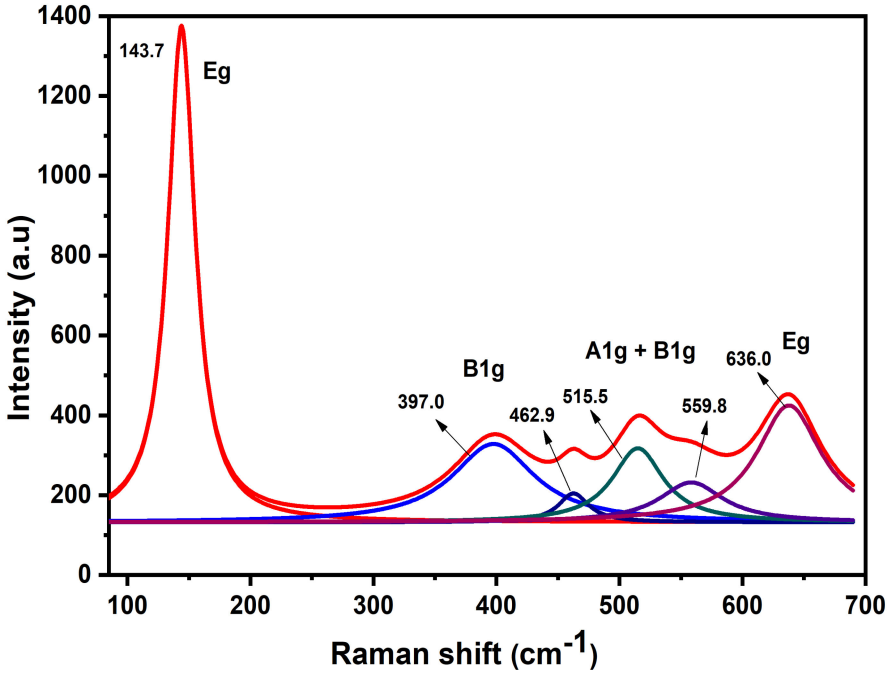

Figure 4. Raman spectroscopy of titanium dioxide nanoparticles.

Figure 5 indicates the CT numbers of the different concentrations of TiO_2-NPs that were scanned. With the addition of NPs concentration, the CT numbers of the solutions improve roughly linearly. The uncertainty of the measurements in the Hounsfield unit (HU) is given by the standard deviation. The CT numbers were ranging from 0 ± 3 HU (without NPs) to 283.7 ± 3 HU (0.235 g/mL). A value of (27.5 ± 3, 75.9 ± 3, 125.7 ± 3, 172.2 ± 3, 235.4 ± 3, and 283.7 ± 3) HU is given by a (0.02, 0.05, 0.1, 0.15, 0.2, 0.235) g/mL concentration of NPs. This concentration is higher than the noise value typically reported by most CT scanners of about 5 HU [37]. These findings show that the existence of TiO_2-NPs even at low concentrations induces observable variations in the scanned media that can be observed on a traditional CT scanner.

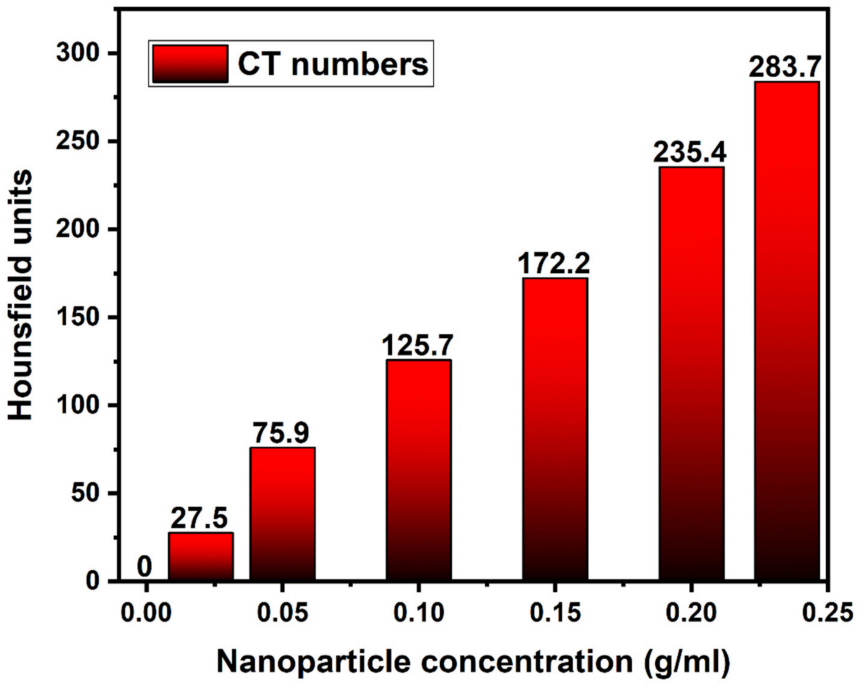

Figure 5. Computed tomography (CT) numbers of TiO_2-NPs solution as a function of concentration.

In Figures 6 and 7, the surface doses are reported as a function of NPs concentration by the EBT2 film pieces. The enhancement is not observed at surface dose for both energies. The measured dose is maximum in both cases only for the solution having no NPs. The measured dose at 50 kVp falls approximately linearly with the concentration of NPs. Changes found during measurements of dose for all concentrations of NPs within 4% of the measurement error for a beam energy of 125 kVp. For the vial that does not contain nanoparticles, none of the obtained values reflects more than 97% of the dose measured. The decrease in surface dose at higher concentrations of NPs can be associated with the absorption of backscattered radiation by the solution of NPs near the surface without a sequential increase in the dose to compensate for this.

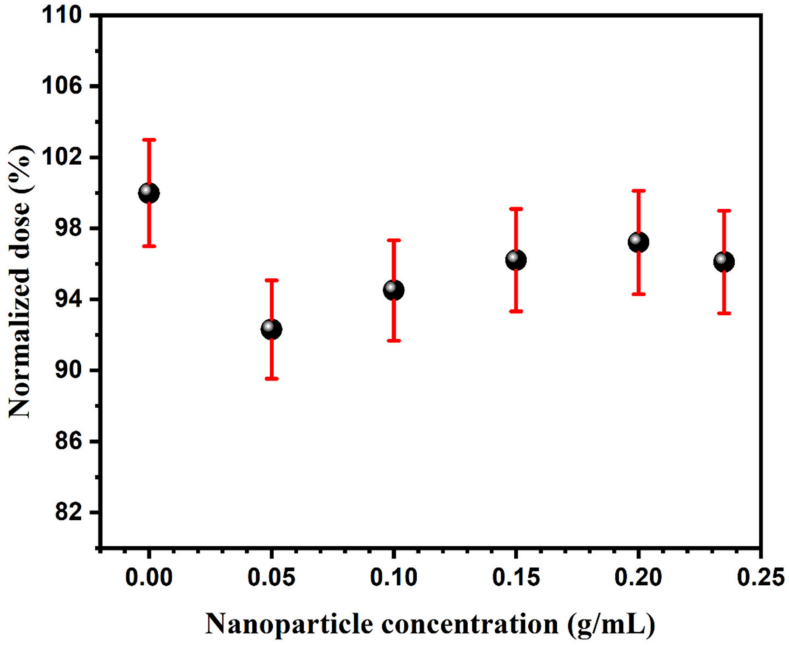

Figure 6. Normalized surface dose as a function of nanoparticle concentration recorded for the 125 kVp radiation beams.

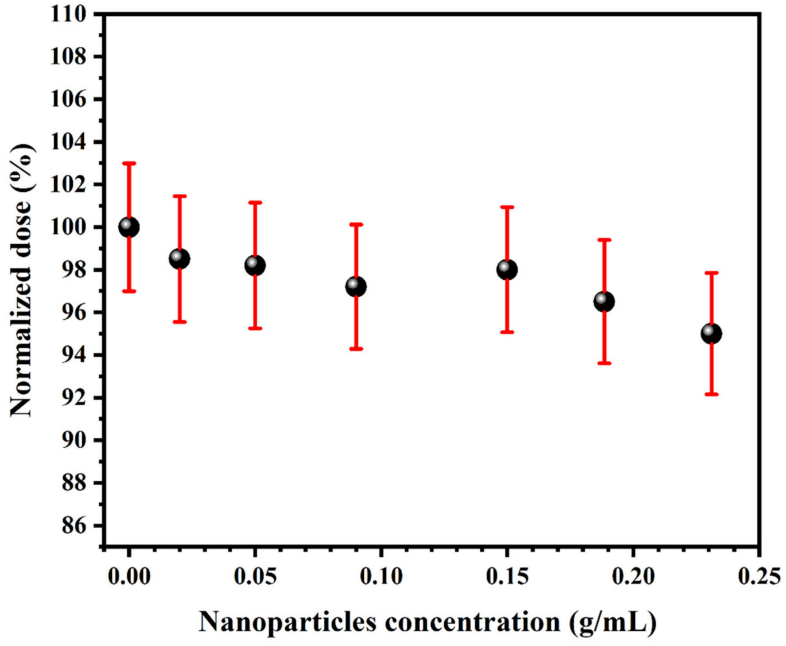

Figure 7. Normalized surface dose as a function of nanoparticle concentration recorded for the 50 kVp radiation beams.

4. Conclusions

TiO_2-NPs were synthesized by the hydrothermal route and used in CT and kilovoltage X-ray unit for contrast enhancement properties. The CT numbers were ranging from 0 ± 3 HU (without NPs) to 283.7 ± 3 HU (0.235 g/mL). For each measurement, the uncertainty is within 3 HU. Our initial findings for titanium dioxide nanoparticles as potential two modes imaging and enhancement agents for therapy suggest that they are a promising contender for image contrast in computed tomography and will be used as a potential anti-tumor agent in drug delivery systems. It has been found that our synthesized highly crystalline unmodified titanium dioxide nanoparticles have an immense potential to improve the existed techniques for cancer imaging and treatment. Bearing impressive results in existing techniques of imaging, there is now increasing curiosity for the potential applications of crystalline unmodified titanium dioxide nanoparticles to radiotherapy and photodynamic therapy. Both of these techniques will bring substantial improvements in the effectiveness of existing cancer treatments in the near future.

Author Contributions: Conceptualization, A.K. and P.A.; methodology, P.A., A.K.; validation, P.A., A.K., S.M. and M.U.K.; formal analysis, A.K., P.A., and S.M.; investigation, A.K., P.A., I.U.D.; resources, P.A., and A.K.; data curation, A.K., P.A., S.M., and M.U.K.; writing—original draft preparation, P.A. and A.K.; writing—review and editing, P.A., A.K., S.M., M.U.K., M.R.I.F., I.U.D., M.A.A., and A.I.A.; visualization, P.A., M.U.K., M.R.I.F., I.U.D., M.A.A., and A.I.A.; supervision, P.A. and S.M.; funding acquisition, M.R.I.F. and M.U.K. All authors have read and agreed to the published version of the manuscript.

Funding: This research was funded by Research Universiti Grant, Universiti Kebangsaan Malaysia, Geran Universiti Penyelidikan (GUP), 2018-134.

Institutional Review Board Statement: Not applicable.

Informed Consent Statement: Not applicable.

Data Availability Statement: Not applicable.

Acknowledgments: We are highly thankful to Prince Sattam Bin Abdulaziz University for providing characterization facilities for our research work.

Conflicts of Interest: The authors declare no conflict of interest.

References

1. Pandey, R.K.; Prajapati, V.K. Molecular and immunological toxic effects of nanoparticles. *Int. J. Biol. Macromol.* **2018**, *107*, 1278–1293. [CrossRef] [PubMed]
2. Bourikas, K.; Kordulis, C.; Lycourghiotis, A. Titanium Dioxide (Anatase and Rutile): Surface Chemistry, Liquid–Solid Interface Chemistry, and Scientific Synthesis of Supported Catalysts. *Chem. Rev.* **2014**, *114*, 9754–9823. [CrossRef] [PubMed]
3. Weir, A.; Westerhoff, P.; Fabricius, L.; Hristovski, K.; Von Goetz, N. Titanium Dioxide Nanoparticles in Food and Personal Care Products. *Environ. Sci. Technol.* **2012**, *46*, 2242–2250. [CrossRef]
4. Swidwinska-Gajewska, A.M.; Czerczak, S. Nanoczastki Ditlenku Tytanu-Dziatanie Biologiczne/Titanium Dioxide Nanoparticles-Biological Effects. *Med. Pr.* **2014**, *65*, 651.
5. Baan, R.; Straif, K.; Grosse, Y.; Secretan, B.; El Ghissassi, F.; Cogliano, V. Carcinogenicity of carbon black, titanium dioxide, and talc. *Lancet Oncol.* **2006**, *7*, 295–296. [CrossRef]
6. Chen, X.-X.; Cheng, B.; Yang, Y.-X.; Cao, A.; Liu, J.; Du, L.-J.; Liu, Y.; Zhao, Y.; Wang, H.-F. Characterization and Preliminary Toxicity Assay of Nano-Titanium Dioxide Additive in Sugar-Coated Chewing Gum. *Small* **2013**, *9*, 1765–1774. [CrossRef]
7. Winkler, H.C.; Notter, T.; Meyer, U.; Naegeli, H. Critical review of the safety assessment of titanium dioxide additives in food. *J. Nanobiotechnol.* **2018**, *16*, 51. [CrossRef]
8. Irshad, M.A.; Nawaz, R.; Rehman, M.Z.U.; Imran, M.; Ahmad, J.; Ahmad, S.; Inam, A.; Razzaq, A.; Rizwan, M.; Ali, S. Synthesis and characterization of titanium dioxide nanoparticles by chemical and green methods and their antifungal activities against wheat rust. *Chemosphere* **2020**, *258*, 127352. [CrossRef]
9. Wang, T.; Weng, Z.; Liu, X.; Yeung, K.W.; Pan, H.; Wu, S. Controlled release and biocompatibility of polymer/titania nanotube array system on titanium implants. *Bioact. Mater.* **2017**, *2*, 44–50. [CrossRef]
10. Yao, C.; Webster, T.J. Anodization: A Promising Nano-Modification Technique of Titanium Implants for Orthopedic Applications. *J. Nanosci. Nanotechnol.* **2006**, *6*, 2682–2692. [CrossRef]

11. Losic, D.; Simovic, S. Self-ordered nanopore and nanotube platforms for drug delivery applications. *Expert Opin. Drug Deliv.* **2009**, *6*, 1363–1381. [CrossRef]
12. De Dicastillo, C.L.; Patiño, C.; Galotto, M.J.; Palma, J.L.; Alburquenque, D.; Escrig, J. Novel antimicrobial titanium dioxide nanotubes obtained through a combination of atomic layer deposition and electrospinning technologies. *Nanomaterials (Basel)* **2018**, *8*, 128. [CrossRef]
13. Al-Swayih, A.A. Electrochemical behavior of self-ordered titania nanotubes prepared by anodization as a promising material for biomedical applications. *J. Am. Sci.* **2014**, *10*, 165–173.
14. Xiao, P.; García, B.B.; Guo, Q.; Liu, D.; Cao, G. TiO_2 nanotube arrays fabricated by anodization in different electrolytes for biosensing. *Electrochem. Commun.* **2007**, *9*, 2441–2447. [CrossRef]
15. Xiao, P.; Zhang, Y.; Cao, G. Effect of surface defects on biosensing properties of TiO_2 nanotube arrays. *Sens. Actuators B Chem.* **2011**, *155*, 159–164. [CrossRef]
16. Sreekantan, S.; Saharudin, K.A.; Wei, L.C. Formation of TiO_2 nanotubes via anodization and potential applications for photocatalysts, biomedical materials, and photoelectrochemical cell. In Proceedings of the IOP Conference Series Materials Science and Engineering 2011, Osaka, Japan, 14–18 November 2010; p. 012002.
17. García-Rodríguez, A.; Vila, L.; Cortés, C.; Hernández, A.; Marcos, R. Effects of differently shaped TiO_2 NPs (nanospheres, nanorods and nanowires) on the in vitro model (Caco-2/HT29) of the intestinal barrier. *Part. Fibre Toxicol.* **2018**, *15*, 33. [CrossRef] [PubMed]
18. Špadina, M.; Gourdin-Bertin, S.; Dražič, G.; Selmani, A.; Dufreche, J.-F.; Bohinc, K. Charge Properties of TiO_2 Nanotubes in $NaNO_3$ Aqueous Solution. *ACS Appl. Mater. Interfaces* **2017**, *10*, 13130–13142. [CrossRef]
19. Akinola, P.; Lateef, A.; Asafa, T.; Beukes, L.; Hakeem, A.; Irshad, H. Multifunctional titanium dioxide nanoparticles biofabricated via phytosynthetic route using extracts of Cola nitida: Antimicrobial, dye degradation, antioxidant and anticoagulant activities. *Heliyon* **2020**, *6*, e04610. [CrossRef]
20. Al-Hadeethi, Y.; Sayyed, M.; Al-Buriahi, M. Bioactive glasses doped with TiO_2 and their potential use in radiation shielding applications. *Ceram. Int.* **2020**, *46*, 14721–14732. [CrossRef]
21. Wang, Y.; Ding, L.; Yao, C.; Li, C.; Xing, X.; Huang, Y.; Gu, T.; Wu, M. Toxic effects of metal oxide nanoparticles and their underlying mechanisms. *Sci. China Mater.* **2017**, *60*, 93–108. [CrossRef]
22. Kandeil, M.A.; Mohammed, E.T.; Hashem, K.S.; Aleya, L.; Abdel-Daim, M.M. Moringa seed extract alleviates titanium oxide nanoparticles (TiO_2-NPs)-induced cerebral oxidative damage, and increases cerebral mitochondrial viability. *Environ. Sci. Pollut. Res.* **2020**, *27*, 19169–19184. [CrossRef]
23. Mesa, A.V.; Norman, A.; Solberg, T.D.; Demarco, J.J.; Smathers, J.B. Dose distributions using kilovoltage x-rays and dose enhancement from iodine contrast agents. *Phys. Med. Biol.* **1999**, *44*, 1955–1968. [CrossRef] [PubMed]
24. Rose, J.H.; Norman, A.; Ingram, M. First experience with radiation therapy of small brain tumors delivered by a computerized tomography scanner. *Int. J. Radiat. Oncol.* **1994**, *30*, 166–167. [CrossRef]
25. Verhaegen, F.; Reniers, B.; Deblois, F.; Devic, S.; Seuntjens, J.; Hristov, D. Dosimetric and microdosimetric study of contrast-enhanced radiotherapy with kilovolt x-rays. *Phys. Med. Biol.* **2005**, *50*, 3555–3569. [CrossRef] [PubMed]
26. Mello, R.S.; Callisen, H.; Winter, J.; Kagan, A.R.; Norman, A. Radiation dose enhancement in tumors with iodine. *Med. Phys.* **1983**, *10*, 75–78. [CrossRef] [PubMed]
27. Kagan, A.R.; Steckel, R.J.; Cancilla, P.; Juillard, G.; Patin, T. The pathogenesis of brain necrosis: Time and dose parameters. *Int. J. Radiat. Oncol.* **1976**, *1*, 729–732. [CrossRef]
28. Cheng, K.; Sano, M.; Jenkins, C.H.; Zhang, G.; Vernekohl, D.; Zhao, W.; Wei, C.; Zhang, Y.; Zhang, Z.; Liu, Y.; et al. Synergistically Enhancing the Therapeutic Effect of Radiation Therapy with Radiation Activatable and Reactive Oxygen Species-Releasing Nanostructures. *ACS Nano* **2018**, *12*, 4946–4958. [CrossRef]
29. Liang, S.; Deng, X.; Xu, G.; Xiao, X.; Wang, M.; Guo, X.; Ma, P.; Cheng, Z.; Zhang, D.; Lin, J. A Novel Pt–TiO_2 Heterostructure with Oxygen-Deficient Layer as Bilaterally Enhanced Sonosensitizer for Synergistic Chemo-Sonodynamic Cancer Therapy. *Adv. Funct. Mater.* **2020**, *30*, 1908598. [CrossRef]
30. Yang, C.-C.; Wang, C.-X.; Kuan, C.-Y.; Chi, C.-Y.; Chen, C.-Y.; Lin, Y.-Y.; Chen, G.-S.; Hou, C.; Lin, F.-H. Using C-doped TiO_2 Nanoparticles as a Novel Sonosensitizer for Cancer Treatment. *Antioxidants* **2020**, *9*, 880. [CrossRef] [PubMed]
31. Su, W.; Wang, H.; Wang, T.; Li, X.; Tang, Z.; Zhao, S.; Zhang, M.; Li, D.; Jiang, X.; Gong, T.; et al. Auger Electrons Constructed Active Sites on Nanocatalysts for Catalytic Internal Radiotherapy. *Adv. Sci.* **2020**, *7*, 1903585. [CrossRef]
32. Garnica-Garza, H. Contrast-enhanced radiotherapy: Feasibility and characteristics of the physical absorbed dose distribution for deep-seated tumors. *Phys. Med. Biol.* **2009**, *54*, 5411–5425. [CrossRef]
33. McMahon, S.J.; Mendenhall, M.H.; Jain, S.; Currell, F. Radiotherapy in the presence of contrast agents: A general figure of merit and its application to gold nanoparticles. *Phys. Med. Biol.* **2008**, *53*, 5635–5651. [CrossRef]
34. Berbeco, R.I.; Ngwa, W.; Makrigiorgos, G.M. Localized Dose Enhancement to Tumor Blood Vessel Endothelial Cells via Megavoltage X-rays and Targeted Gold Nanoparticles: New Potential for External Beam Radiotherapy. *Int. J. Radiat. Oncol.* **2011**, *81*, 270–276. [CrossRef] [PubMed]
35. Chithrani, D.B.; Jelveh, S.; Jalali, F.; Van Prooijen, M.; Allen, C.; Bristow, R.G.; Hill, R.P.; Jaffray, D.A. Gold Nanoparticles as Radiation Sensitizers in Cancer Therapy. *Radiat. Res.* **2010**, *173*, 719–728. [CrossRef] [PubMed]

36. Anshup; Venkataraman, J.S.; Subramaniam, C.; Kumar, R.R.; Priya, S.; Kumar, T.R.S.; Omkumar, R.V.; John, A.; Pradeep, T. Growth of Gold Nanoparticles in Human Cells. *Langmuir* **2005**, *21*, 11562–11567. [CrossRef]
37. Guy, C.; Ffytche, D. *An Introduction to the Principles of Medical Imaging*; Imperial College Press: London, UK, 2005.
38. Schladt, T.D.; Schneider, K.; Shukoor, M.I.; Natalio, F.; Bauer, H.; Tahir, M.N.; Weber, S.; Schreiber, L.M.; Schröder, H.C.; Müller, W.E.G.; et al. Highly soluble multifunctional MnO nanoparticles for simultaneous optical and MRI imaging and cancer treatment using photodynamic therapy. *J. Mater. Chem.* **2010**, *20*, 8297–8304. [CrossRef]
39. Huang, W.-Y.; Davis, J.J. Multimodality and nanoparticles in medical imaging. *Dalton Trans.* **2011**, *40*, 6087–6103. [CrossRef] [PubMed]
40. Podgorsak, E.B.; Kainz, K. Radiation Oncology Physics: A Handbook for Teachers and Students. *Int. At. Energy Agency* **2006**, *33*, 1920. [CrossRef]
41. Schultz, B.-J.; Wust, P.; Lüdemann, L.; Jost, G.; Pietsch, H. Monte Carlo simulation of contrast-enhanced whole brain radiotherapy on a CT scanner. *Med. Phys.* **2011**, *38*, 4672–4680. [CrossRef] [PubMed]
42. Ungun, B.; Prud'Homme, R.K.; Budijono, S.J.; Shan, J.; Lim, S.F.; Ju, Y.; Austin, R. Nanofabricated up conversion nanoparticles for photodynamic therapy. *Opt. Express* **2008**, *17*, 80–86. [CrossRef]
43. Goktas, A. High-quality solution-based Co and Cu co-doped ZnO nanocrystalline thin films: Comparison of the effects of air and argon annealing environments. *J. Alloys Compd.* **2018**, *735*, 2038–2045. [CrossRef]
44. Muilenberg, G. *Handbook of X-ray Photoelectron Spectroscopy*; Perkin-Elmer Corporation: Waltham, MA, USA, 1979; Volume 64.
45. Göpel, W.; Anderson, J.A.; Frankel, D.; Jaehnig, M.; Phillips, K.; Schäfer, J.A.; Rocker, G. Surface defects of TiO_2 (110): A combined XPS, XAES AND ELS study. *Surf. Sci.* **1984**, *139*, 333. [CrossRef]
46. Warren, D.S.; Shapira, Y.; Kisch, H.; McQuillan, A.J. Apparent Semiconductor Type Reversal in Anatase TiO_2 Nanocrystalline Films. *J. Phys. Chem. C* **2007**, *111*, 14286–14289. [CrossRef]
47. Wang, L.-Q.; Baer, D.; Engelhard, M.H.; Shultz, A. The adsorption of liquid and vapor water on TiO_2(110) surfaces: The role of defects. *Surf. Sci.* **1995**, *344*, 237–250. [CrossRef]
48. Bullock, E.; Patthey, L.; Steinemann, S. Clean and hydroxylated rutile TiO_2(110) surfaces studied by X-ray photoelectron spectroscopy. *Surf. Sci.* **1996**, *504*, 504–510. [CrossRef]
49. Choudhury, B.; Dey, M.; Choudhury, A. Defect generation, d-d transition, and band gap reduction in Cu-doped TiO_2 nanoparticles. *Int. Nano Lett.* **2013**, *3*, 25. [CrossRef]
50. Choudhury, B.; Choudhury, A. Room temperature ferromagnetism in defective TiO_2 nanoparticles: Role of surface and grain boundary oxygen vacancies. *J. Appl. Phys.* **2013**, *114*, 203906. [CrossRef]
51. Frank, O.; Zukalova, M.; Laskova, B.; Kürti, J.; Koltai, J.; Kavan, L. Raman spectra of titanium dioxide (anatase, rutile) with identified oxygen isotopes (16, 17, 18). *Phys. Chem. Chem. Phys.* **2012**, *14*, 14567–14572. [CrossRef]
52. Li, F.; Gu, Y. Improvement of performance of dye-sensitized solar cells by doping Er_2O_3 into TiO_2 electrodes. *Mater. Sci. Semicond. Process.* **2012**, *15*, 11–14. [CrossRef]
53. Salis, M.; Ricci, P.C.; Anedda, A. An analytical form for the Raman shift dependence on size of nanocrystals. *J. Raman Spectrosc.* **2009**, *40*, 64–66. [CrossRef]